Check for updates

Energy Technology
Generation, Conversion, Storage, Distribution
www.entechnol.de

Energy Harvesting by V-Shape Bluff Bodies with Various Apical Angles Attached to a Revolute Joint

Musa Özkan, Sinan Basaran, and Onur Erkan*

This study parametrically investigates the efficiency of an integrated energy harvesting system that consists of a piezoelectric patch attached to a cantilever beam and V-shape bluff bodies with various apical angles. V-shape bluff bodies are connected to a cantilever beam with a revolute joint that represents a two degrees-of-freedom configuration. The mechanical energy of the galloping and fluttering motions, resulting from the vortex shedding that appears downstream of the bluff bodies, is converted into electricity by means of a piezoelectric patch. The apical angle of the V-shape geometries, that varies between 0° and 180°, is the main parameter where the generated voltages and the related power curves are the major results for the evaluation of the efficiency of this harvesting system. Based on the experimental examinations, the maximum output power of 0.295 mW is produced at a wind speed of 10 m s^{-1} for the apical angle of 180° and the electrical resistance of 230 kΩ. Moreover, the proposed energy harvester system can still produce usable output power for the apical angles ranges from 0° to 20° and from 170° to 180°.

1. Introduction

The twenty-first century is already turning out to be the century of the energy crisis. In addition, with the rapid technological progress, many low-power devices, especially wireless devices, sensors, embedded medical devices, and other microelectromechanical systems, have become a part of our daily lives. Although chemical batteries seem like a suitable method to meet this increasing energy need, the importance of self-powered devices is increasing due to the environmental concerns in the long term. The toxic effect of the chemical batteries can contaminate water supplies and ecosystems if they leach out of the trash yard. Therefore, the energy conversions obtained from ambient vibrations and flow-induced movements are of great importance.

The most popular energy conversion method obtained from flow-induced vibrations is the integration of piezoelectric materials into systems.[1–9] In addition, hybrid systems, created using piezoelectric materials together with other systems such as electromagnetic devices, increase the performance obtained from energy harvesting.[10–13] Moreover, triboelectric nanogenerators have shown a great potential as a means of novel energy harvesting devices.[14,15] Piezoelectric materials are basically used as a patch by mounting on a beam element with a fixed support.[16–18] With the oscillation created by flow-induced vibrations, electrical voltage can be collected over the piezoelectric patch. Flow-induced energy harvesting systems cover a linkage of three different research areas, which are fluid dynamics, structural design, and electricity implementation.[19] Related studies between these main research topics show the incremental improvement and methodology of the energy harvesters by means of flow-induced vibrations.[20] This popular energy harvesting method has been studied by many researchers and groups.[21–25] The main purpose of these studies is to increase the efficiency of the energy harvesting systems based on flow-induced vibrations and thus ensure sustainability.

In order to increase the amount of energy obtained from the piezoelectric material, the vibrational motions need to be increased. The most common way of increasing these motions is the application of bluff-body geometries, which are fixedly mounted on the beam element.[23–28] Kim et al.[29] proposed a novel piezoelectric energy harvester based on coupled transverse and interference galloping to improve the energetic performance of the galloping-based piezoelectric energy harvester system. A hybrid piezoelectric–electromagnetic energy harvester was investigated by Muthalif et al.[30] where a bluff body was used as a harvester which has vibrational motions resulting from vortices that appear around this body. They performed an experimental study by gluing the piezoelectric patch onto a beam element to convert the mechanical strain into electricity.

Bluff-body geometries as energy harvesters can be designed in various shapes. The most important feature of these designs is that the bluff body needs to be created as aerodynamically beneficial to acquire most of the kinetic energy present in the flow around the model. Bell-shaped and horn-shaped cylinder geometries were investigated by Wang et al.[31] to show the effects of ash deposition on a wake galloping energy harvester. The effects of dissimilar wakes on the energy harvesting of flow-induced vibrations were investigated by Tamimi et al.[32] They proved that the dissimilar square wake could increase the harvested mechanical power of the circular oscillator. Yan et al.[33] proposed a highway wind flow exploitation energy harvesting system supported with tandem cylinders using a wake-induced vibration effect.

M. Özkan, S. Basaran, O. Erkan
Faculty of Engineering
Department of Mechanical Engineering
Bilecik Seyh Edebali University
Bilecik 11210, Türkiye
E-mail: musa.ozkan@bilecik.edu.tr

The ORCID identification number(s) for the author(s) of this article can be found under https://doi.org/10.1002/ente.202300579.

DOI: 10.1002/ente.202300579

 © 2023 Wiley-VCH GmbH

21944296, 0, Downloaded from https://onlinelibrary.wiley.com/doi/10.1002/ente.202300579 by Bilecik Seyh Edebali, Wiley Online Library on [22/08/2023]. See the Terms and Conditions (https://onlinelibrary.wiley.com/terms-and-conditions) on Wiley Online Library for rules of use; OA articles are governed by the applicable Creative Commons License

They conducted the experimental study with a piezoelectric beam and cylinder-shaped bluff-body geometries to show that upstream-wise spacing is crucial for the wind energy harvesting.

It has been investigated that various modifications made on known bluff-body geometries such as rectangular shapes have an effect on the energy harvesting performance. Wang et al.,[34] for instance, proposed an experimental study to show the influences of different metasurfaces on the aerodynamic characteristics of bluff bodies. The results show that the modification on the surface of the harvesters can significantly change the aerodynamic behavior of the bluff body. Thus, it can be beneficial to the performance of a galloping energy harvester.

Another stunning field of study in energy harvesting systems is parametric study applications. There are studies obtained by parameterizing the bluff-body geometries used for different structural dimensions. Chen et al.[35] conducted a study for energy harvesting from vibration responses of cylinders with different diameters. They have presented an experimental setup and parametric vibration study for energy harvesting from flow-induced vibrations of a flexibly connected cylinder geometry in the wake of another cylinder with a smaller diameter. Zhu et al.[36] conducted an experimental and numerical study for investigating the effects of the angle of attack and the length ratio of a trapezoidal oscillator on its energy harvesting performance. They parametrized the length of the longer base and the height of the shorter base of the considered oscillators for different angles of attack of the incoming flow. Changes in the inclination angle of the circular cylinder with respect to incoming flow in order to broaden the effective wind speed bandwidth of the piezoelectric energy harvester were investigated by researchers.[37] Energy harvesting characteristics of the system under different inclination angles were proposed and results were supported by the experimental study. The cylinder with a certain inclination angle was obtained, which could effectively increase the torsional vibration within a certain range of the wind speed, thus resulting a high voltage output.

Hitherto, the preceding studies reveal the importance of the energy harvesting system and highlight the importance of increasing the amount of energy obtained. In the present study, a piezoelectric energy harvesting system with a V-shape bluff-body geometry was parametrically investigated. The proposed bluff body has a V-shape geometry with an apical angle (θ) which varies from 0° to 180°. These V-shape bluff bodies, which are produced for 22 different apical angles, have been experimentally studied.

The original point of the current work is that the bluff-body geometries are attached to the fixed-support beam in an unconventional way. Usually, a fixed-joint approach is used for bluff-body geometries, with a mechanical attachment on the beam. However, in this study, it is aimed to enable the bluff-body geometries to rotate freely on the beam using the revolute joint approach, that is the energy harvesting system represents a two degrees-of-freedom configuration. This implementation in this research follows the original and novel studies[38,39] where a small flap was connected to a cantilevered piezoelectric beam by a revolute joint. Thus, by means of the vortices downstream of the geometry, the V-shape harvester models start to oscillate around this revolute joint related to vortex shedding. This oscillating model around the revolute joint and the piezoelectric patch attached to the cantilever beam positively increase the amount of collected energy from the harvesting system. Furthermore, V-shape harvester geometries are also attached to the cantilever beam with fixed support to compare and thus demonstrate the eligibility of the proposed V-shape harvesters with a revolute joint.

The rest of this article is organized as follows. In Section 2, the integrated motion characteristics of the galloping–fluttering energy harvester system are defined. Subsequently, the experimental facility of the V-shape energy harvester system is presented in Section 3 to show the effects of the various apical angles attached to a revolute joint on energy harvesting performance. In Section 4, experimental results are demonstrated for all V-shape geometries with an apical angle (θ) which varies from 0° to 180°. Finally, in the last section, a detailed decision and conclusion are performed to show the performance of the proposed energy harvesting system for different configurations.

2. Integrated Galloping–Fluttering Energy Harvester

Cross flows over bluff bodies are prone to instabilities due to the disturbances resulting from the sharp edges of these geometries. These disturbances then form downstream vortices in the wake of the bluff bodies, which is called a well-known flow phenomenon of the Kármán vortex street. Once the freestream flow velocity over the bodies exceeds a critical threshold, the periodic shedding of these Kármán vortex structures provokes the pressure field around the surface of the bluff body to become periodic. This periodicity of the pressure on the surface induces periodic aerodynamic forces on the geometries. These bodies under periodic forces then start to oscillate in the transverse direction to the flow, supposing that the motion of the body in the parallel direction to the flow is restricted. If this motion presents low frequencies and large amplitudes, this motion of the bluff body is usually called galloping. This flow configuration is somewhat exemplified in this present study by the proposed experimental setup.

Bluff bodies subject to such cross flows represent a typical example of energy harvesting mechanisms where these configurations are called galloping energy harvesters. The general application of the galloping-type energy harvesters is that a prismatic bluff body is attached to the end of a cantilever beam where the maximum amplitude is aimed which is related with a higher lifting force acting on the body.[40] However, in the current study, a different type of application has been implemented by means of the use of a revolute joint which extends the degree of freedom of the whole harvester system with an additional free rotational movement. As a result of this increased degree of freedom, the attached bluff body represents a flutter type of vibrational movement at the end of the cantilever beam, in addition to the galloping movement of the complete harvester system. By this means, an integrated galloping–fluttering harvester system is introduced and the governing equations of the system with electromagnetic coupling are given by Equation (1)–(3)

$$M\ddot{x} + C\dot{x} + Kx - \Theta C_p^{-1} q = F_{\mathrm{L}} \cos(\alpha - \varphi) + F_{\mathrm{D}} \sin(\alpha - \varphi) \quad (1)$$

© 2023 Wiley-VCH GmbH

$$J\ddot{\varphi} + C_t\dot{\varphi} + K_t\varphi = \tau + F_L r\cos\alpha + F_D r\sin\alpha \quad (2)$$

$$R\dot{q} - C_p^{-1}\Theta^T x + C_p^{-1}q = 0 \quad (3)$$

Here, x is the response lateral displacement, φ is the response angular displacement, and M represents the useful mass of the energy harvester system which can be calculated as $M = (33/140)$ $M_b + M_{tip}$. Here, M_b and M_{tip} indicate the masses of the beam and the bluff body, respectively.[1,41] Moreover, in Equation (2), J indicates the equivalent inertia moment of the energy harvester; C and C_t represents the viscous damping coefficients of the beam element. The stiffnesses of this beam element for lateral and angular directions are also represented by K and K_t, respectively. The term R represents the electrical resistance, C_p corresponds to the piezocapacitance matrix, Θ denotes the electromechanical coupling matrix, and q is the output charge. The symbol r in Equation (2) represents the distance between the center of pressure and the joint. F_L and F_D are the lift and drag forces, respectively, acting on the harvester geometry that are given by Equation (4) and (5) as

$$F_L = \frac{1}{2}\rho\, U_\infty^2\, A\, C_L(\alpha) \quad (4)$$

$$F_D = \frac{1}{2}\rho\, U_\infty^2\, A\, C_D(\alpha) \quad (5)$$

Here, ρ and U_∞ are the density and the freestream velocity of the air. Moreover, C_L and C_D are the lift and drag coefficients that are the normalized measures of the lift force and the drag force acting on the V-shape bluff bodies regardless of their size, shape, and orientation.[42] Information about how these coefficients vary with the angle of attack can be obtained from static experiments.[43] Furthermore, A is the cross-sectional area of the bluff body facing the freestream airflow. Finally, τ is the moment acting on the bluff body with respect to the revolute joint that is given by Equation (6) where C_M indicates the moment coefficient and w_a is the width of the harvester geometry.

$$\tau = \frac{1}{2}\rho\, U_\infty^2\, A\, w_a\, C_M(\alpha) \quad (6)$$

The dynamics of the traditional energy harvesting devices are usually expressed with a single degree of freedom, whereas the currently introduced approach in this study adds an extra degree of freedom to the system due to the implementation of the revolute joint.

3. Experimental Section

The experimental facility consisted of an airflow tunnel where the maximum airflow velocity of 10 m s^{-1} can be reached. The air was driven by an axial fan with a power of 235 W and a flow rate of 8,000 m^3 h^{-1} in this suction-type, low-speed, and open-circuit wind tunnel. The first component of the tunnel in the direction of the flow was the collector that had a 0.65 m length and a contraction ratio of 6.25. A wire mesh screen was also attached to the entrance of this collector to keep the turbulence intensity levels below 3%. The diameter of the wire was 1 mm, which formed rectangular cross sections of 13 × 13 mm. The test section of the tunnel had a rectangular cross-sectional area of 300 × 300 mm that was 0.85 m in length. The prototype was placed in the middle of the test section, that is, 1.05 m downstream of the flow. The test section and the related experimental equipment are shown in **Figure 1**. The airflow left the wind tunnel through a diffuser with a length of 1.65 m and a divergence angle of 7°. The airflow velocity was measured by Testo 405i hot-wire anemometer. An aluminum beam was assembled via fixed support at the channel floor, as shown in Figure 1 and **Figure** 2, which constituted a cantilever beam. The piezoelectric (PZT)

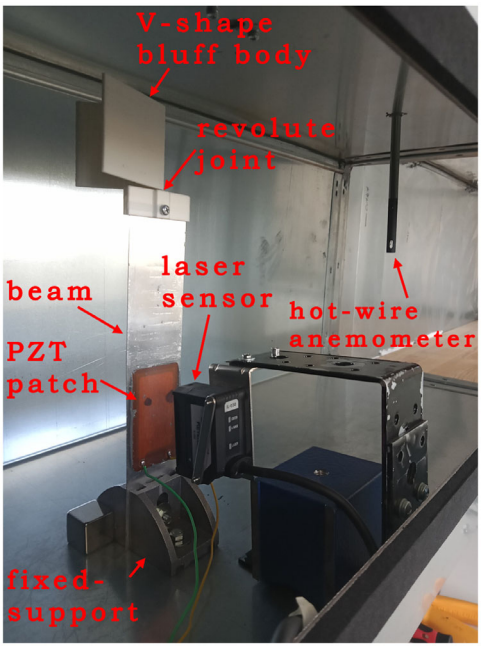

Figure 1. The experimental facility consists of an airflow tunnel, a V-shape harvester with attachments and sensors.

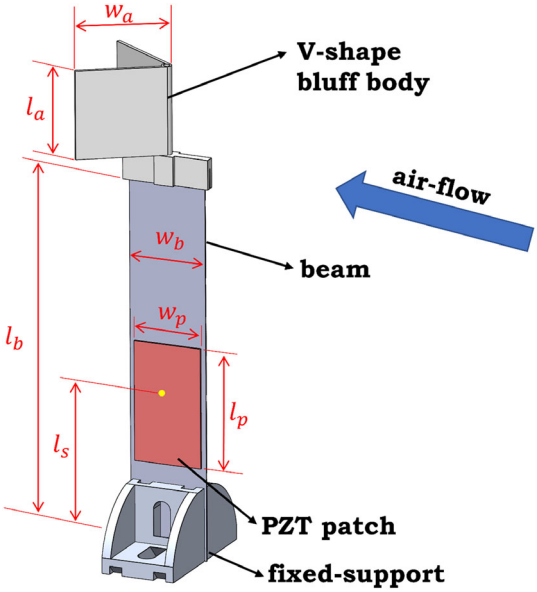

Figure 2. The illustration of the harvester system immersed in airflow.

© 2023 Wiley-VCH GmbH

21944296, 0, Downloaded from https://onlinelibrary.wiley.com/doi/10.1002/ente.202300579 by Bilecik Seyh Edebali, Wiley Online Library on [22/08/2023]. See the Terms and Conditions (https://onlinelibrary.wiley.com/terms-and-conditions) on Wiley Online Library for rules of use; OA articles are governed by the applicable Creative Commons License

patch attached to the cantilever beam was used to convert the mechanical energy of the galloping motion to electrical energy. The AC voltages produced by this PZT patch were read by means of AATech ADS-3102B oscilloscope. In addition, the displacement of the cantilever beam was measured by a laser displacement sensor and a V-Daq RT-4 data acquisition system.

The bluff body had a V-shape with an apical angle (θ) which varied from 0° to 180°. The height and the width of the body were 45 and 45 mm, respectively, and the thickness was 2 mm. There were 22 bluff bodies used in this study, which are displayed in **Figure 3**. Both the revolute and fixed joint cases were tested, as shown in **Figure 4**. Moreover, the experiments were performed for the angles of attack (α) of 0°, 10°, and 20°, which stated the angle between the flow direction and the beam. Eight values of electrical resistance, which varied between 1 and 2.200 kΩ, were used in order to obtain power curves. Both the dimensions of the experimental setup and the tested parameters are listed in **Table 1**.

First, the bluff bodies which had the apical angles of 0° and 10° were investigated for the airflow velocities of 9.3 and 10 m s^{-1} which, respectively, corresponded to $Re = 2.95 \times 10^4$ and $Re = 3.16 \times 10^4$. Here the Reynolds number was defined in a usual way as $Re = U_\infty l_a/\nu$. By this means, the susceptibility of the harvester system to Reynolds number was observed and thus a preferable flow condition could be obtained to have a prompt and continuous galloping motion. Subsequently, both the fixed and the revolute joint cases with the apical angles of 0°, 170°, and 180° were tested at $Re = 3.16 \times 10^4$.

In consequence of the obtained results, which will be mentioned in the following section, it was decided that the experiments were conducted just for the revolute joint cases. Both the AC voltage output and the displacement of the beam were measured simultaneously during the experiments. Once the voltage results were acquired for all cases without resistors, the voltage outputs with different values of electrical resistance

Table 1. The dimensions of the experimental setup and tested parameters.

Name	Symbol	Value	Unit
The width of PZT patch	w_p	35	mm
The height of PZT patch	l_p	61	mm
The width of beam	w_b	41	mm
The height of beam	l_b	200	mm
The thickness of beam	t_b	0.5	mm
The height of laser sensor	l_s	60	mm
The width of harvester	w_a	45	mm
The height of harvester	l_a	45	mm
The apical angle of harvester	θ	0, 10, 20, 30, 40, 50, 55, 60, 65, 70, 80, 90, 100, 110, 120, 130, 140, 150, 160, 165, 170, 180	°
The angle of attack	α	0, 10, 20	°
Electrical resistance	R	1, 3.3, 22, 100, 330, 1000, 1500, 2200	kΩ

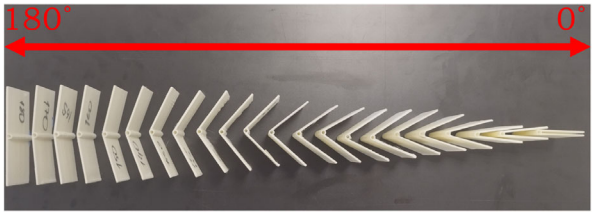

Figure 3. Bluff bodies with various apical angles used in the experiments.

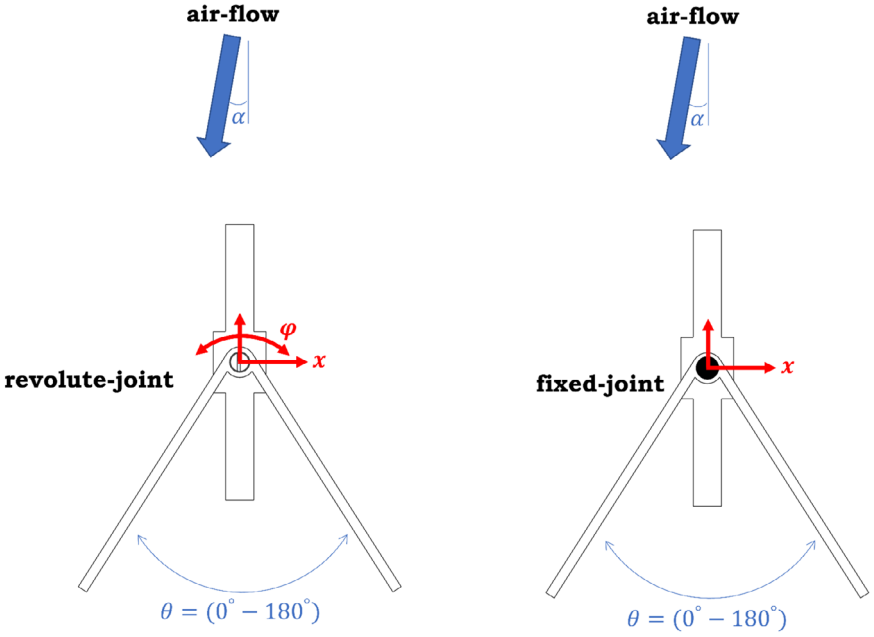

Figure 4. Fixed and revolute joints with parameters of apical angles and the angle of attack.

© 2023 Wiley-VCH GmbH

21944296, 0, Downloaded from https://onlinelibrary.wiley.com/doi/10.1002/ente.202300579 by Bilecik Seyh Edebali, Wiley Online Library on [22/08/2023]. See the Terms and Conditions (https://onlinelibrary.wiley.com/terms-and-conditions) on Wiley Online Library for rules of use; OA articles are governed by the applicable Creative Commons License

were obtained in order to generate the power curves of the energy harvesting system.

4. Results and Discussion

Figure 5 displays the comparison of the onset of the oscillations of the V-shape harvester with the apical angle of $\theta = 0°$ at $Re = 2.95 \times 10^4$ (black solid line) and $Re = 3.16 \times 10^4$ (red dashed line). These oscillations for both Reynolds numbers are obtained at the zero angle of attack, $\alpha = 0°$. The x-axis, here, represents the flow time in seconds and the y-axis shows the generated AC voltages from the piezoelectric patch. To obtain these results, the V-shape harvesters attached to a cantilever beam with a revolute joint are kept fixed where there exists a fully developed uniform airflow over them with two different velocities corresponding to the specified Reynolds numbers. The harvesters are then released to generate galloping motions, which are induced by the airflow. The starting time shown in this figure ($t = 0$) is the instantaneous moment when the harvesters are set free. It can clearly be seen in this figure that the V-shape harvester geometry starts a continuous oscillation at around $t = 4$ s for $Re = 3.16 \times 10^4$. On the other hand, when $Re = 2.95 \times 10^4$, some vibrational motions are seen at $t = 1.2$ s and $t = 4.6$ s. However, a constant oscillation cannot be acquired until around $t = 7$ s at this Reynolds number.

The onset constitution of the V-shape harvesters is also compared for the apical angle of $\theta = 10°$ and the comparison is illustrated in **Figure 6**. Similar to the $\theta = 0°$ harvester, the response time of the $\theta = 10°$ harvester is far less at $Re = 3.16 \times 10^4$ than $Re = 2.95 \times 10^4$. The start of the constant oscillation now seems to be immediate at $\approx t = 1$ s for $Re = 3.16 \times 10^4$ whereas it is around $t = 6.2$ s for $Re = 2.95 \times 10^4$. For both apical angles, the steady-state oscillations are observed earlier at the wind speed of 10 m s^{-1}, corresponding to $Re = 3.16 \times 10^4$. Moreover, for the wind speeds below 9.3 m s^{-1}, this proposed harvester system barely oscillates, that is, the cut-in velocity for the system can be considered as $\approx$9.3 m s^{-1}. Furthermore, V-shaped bluff bodies can provide immediate limit-cycle oscillations and thus the time to reach a steady-state condition is much shorter compared to the flat plates ($\theta = 0°$ and $\theta = 180°$), as shown in Figure 5 and Figure 6.

Based on the results shown in Figure 5 and Figure 6 all of the following results in this study were obtained at $Re = 3.16 \times 10^4$, that is, the airflow velocity of 10 m s^{-1}, since the Kármán vortex street seems to form quicker, which results in the galloping of the harvester attached to a revolute joint.

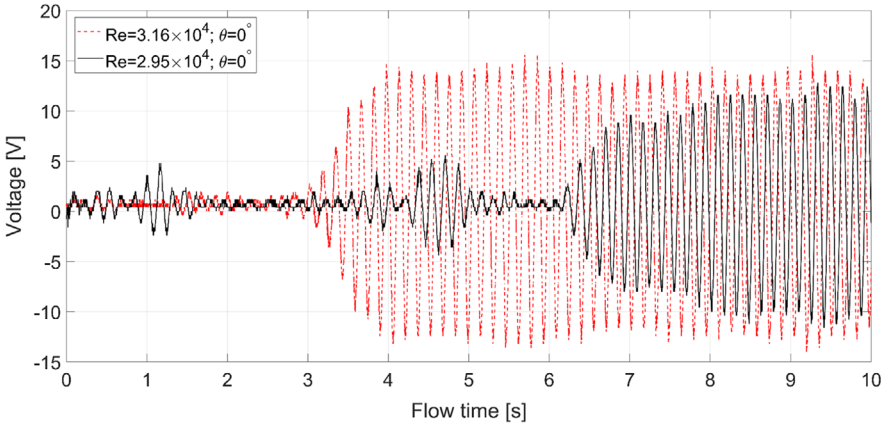

Figure 5. The onset of oscillations of the V-shape revolute joint harvester with $\theta = 0°$.

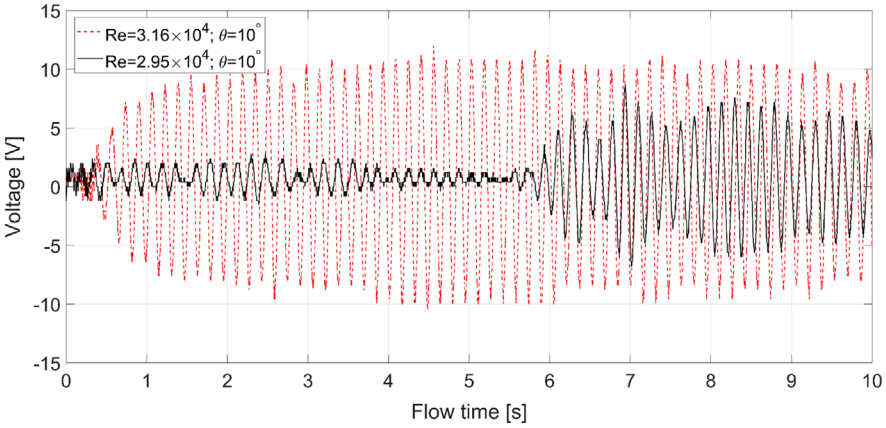

Figure 6. The onset of oscillations of the V-shape revolute joint harvester with $\theta = 10°$.

© 2023 Wiley-VCH GmbH

21944296, 0, Downloaded from https://onlinelibrary.wiley.com/doi/10.1002/ente.202300579 by Bilecik Seyh Edebali, Wiley Online Library on [22/08/2023]. See the Terms and Conditions (https://onlinelibrary.wiley.com/terms-and-conditions) on Wiley Online Library for rules of use; OA articles are governed by the applicable Creative Commons License

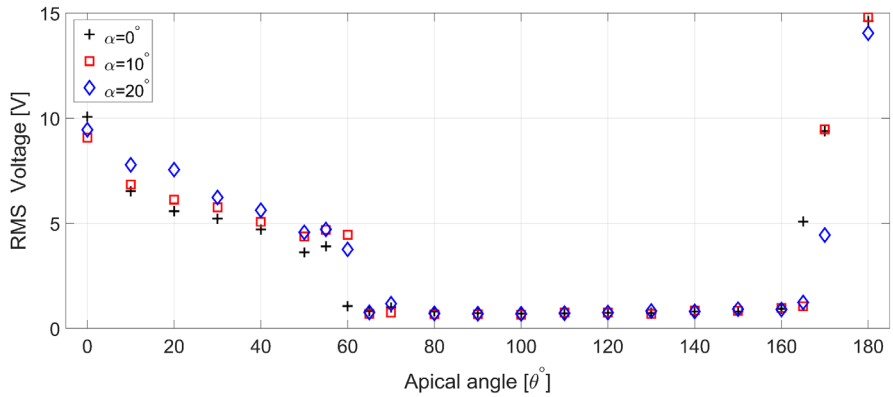

Figure 7. RMS values of voltages at various apical angles ranging from $\theta = 0°$ to $\theta = 180°$ at different angles of attack; $\alpha = 0°$, $\alpha = 10°$, $\alpha = 20°$.

The root-mean-square (RMS) values of AC voltages generated by means of the piezoelectric patch at three different angles of attack $\alpha = 0°$, $\alpha = 10°$, $\alpha = 20°$ and for various apical angles ranging from $\theta = 0°$ to $\theta = 180°$ are shown in **Figure 7**. The very first significant aspect that can clearly be seen in this figure is that there is an ineffective region between $\theta = 65°$ and $\theta = 160°$. Between these apical angles, there are almost no oscillations of the harvesters. The harvester with $\theta = 180°$, which represents a flat plate perpendicularly positioned to the airflow, seems to be the most beneficial model in terms of its capability of producing electricity. This most advantageous design is followed by the harvesters with $\theta = 0°$ (a flat plate parallel to the airflow) and $\theta = 170°$.

Furthermore, the electricity production appears to be reduced with an increase in the apical angle until around $\theta = 60°$ for $\alpha = 0°$ and $\theta = 65°$ for $\alpha = 10°$ and $\alpha = 20°$. After these transitional apical angles, the oscillation of the harvester and thus the production of electricity is suddenly stopped and an ineffective region begins. This region continues to until around $\theta = 165°$ for $\alpha = 0°$ and $\theta = 170°$ for $\alpha = 10°$ and $\alpha = 20°$.

One of the main motivations of this study is that the proposed V-shape harvesters are not susceptible to the direction of the airflow. In other words, by means of the revolute joint, the harvester geometry can spontaneously be orientated toward the airflow. Results displayed in Figure 7 support this motivation because the transitional apical angle is postponed to $\theta = 65°$ when the airflow is directed accordingly to have the angles of attack of $\alpha = 10°$ and $\alpha = 20°$.

To better understand the insights of the oscillations characteristics at the transitional apical angle ($\theta = 60°$), the produced voltages are compared for two different angles of attack, which are $\alpha = 0°$ and $\alpha = 20°$, in **Figure 8**. This figure displays the voltage outcomes resulting from the vibrational motion of the system between the flow time of 4 and 10 s. The results are clearly distinguishable as there exists a constant galloping motion when the angle of attack is set to $\alpha = 20°$. However, the galloping motion seems to be irregular at $\alpha = 0°$. The harvesting system operates unpredictably at this angle of attack as the flow-induced oscillations stop and start suddenly and randomly. Conclusively, it can be stated that at this specific transitional apical angle of 60°, accordingly orientated airflow, that is, airflow approaching to the system with $\alpha = 20°$, can be beneficial to the proposed harvester system.

Figure 9 illustrates the comparison of the voltages produced by means of the fixed and revolute joints at the apical angle of $\theta = 180°$. The harvester element with this angle represents a flat plate perpendicularly placed in the airflow when its connection to the cantilever beam is made by a fixed joint. On the other hand,

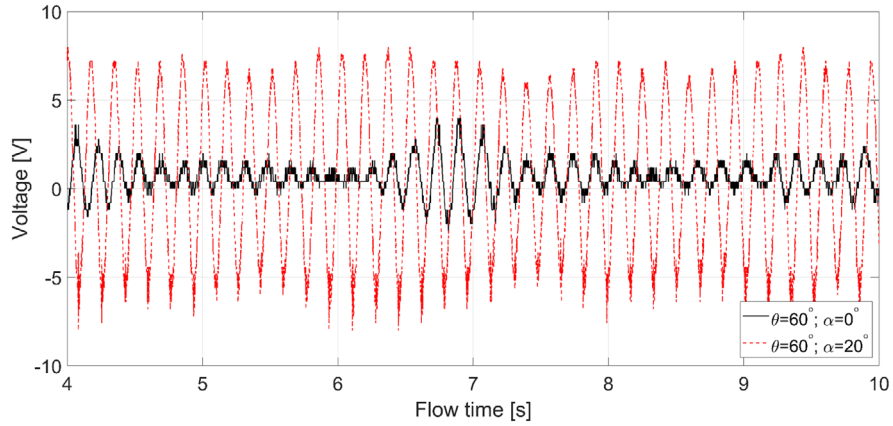

Figure 8. Voltage readings for the transitional apical angle of ($\theta = 60°$) at $\alpha = 0°$ and $\alpha = 20°$.

© 2023 Wiley-VCH GmbH

21944296, 0, Downloaded from https://onlinelibrary.wiley.com/doi/10.1002/ente.202300579 by Bilecik Seyh Edebali, Wiley Online Library on [22/08/2023]. See the Terms and Conditions (https://onlinelibrary.wiley.com/terms-and-conditions) on Wiley Online Library for rules of use; OA articles are governed by the applicable Creative Commons License

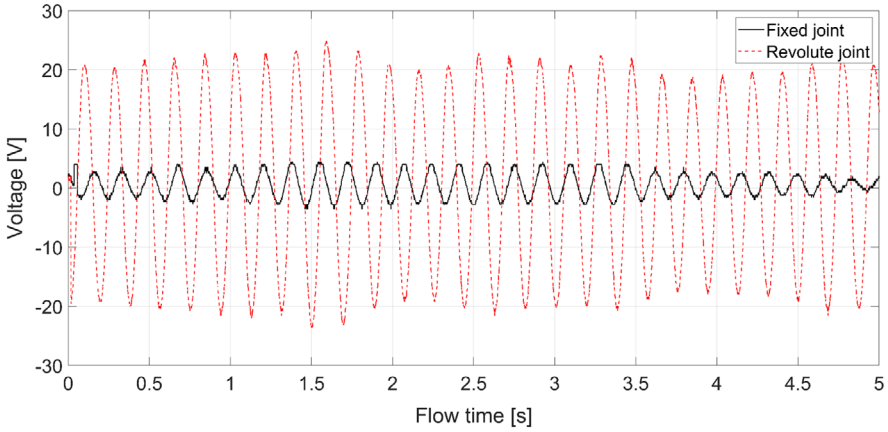

Figure 9. The comparison of the voltages produced by fixed and revolute joints at $\theta = 180°$.

when the connection is obtained by a revolute joint, this flexibility results in a more effective system in terms of its electricity production. This phenomenon similarly occurs at the apical angle of $\theta = 0°$, as shown in **Figure 10**. This is a flat plate with 5 mm thickness that is positioned parallel to the airflow where there are flow separation and thus the Kármán vortices. Nevertheless, the galloping oscillations resulting from these vortices seem to be diminutive with a fixed joint connection. However, once a revolute joint is used, the oscillation of the harvester system is significantly increased.

The power equation obtained, when the RMS voltage (V) scavenged by a piezoelectric element is passed over an electrical resistance (R), can be expressed by Equation (5) as follows

$$P_{\text{piezoelectric}} = \frac{V^2}{R} \tag{7}$$

Figure 11 displays the acquired electrical energy from the harvester system with the application of eight different values of electrical resistance (R), which are 1 kΩ, 3.3 kΩ, 22 kΩ, 100 kΩ, 330 kΩ, 1 MΩ, 1.5 MΩ, and 2.2 MΩ. The obtained power curves for these loads are presented for the three apical angles ($\theta = 0°$, 55°, 180°) and for three angles of attack ($\alpha = 0°$, 10°, 20°). One obvious observation is that the harvester geometry with $\theta = 180°$ produces the maximum power value of ≈0.295 mW at ≈230 kΩ. This power output seems to be comparable to those reported in literature by several approaches to energy harvesting at similar wind speed values. Wang et al.,[44] for instance, proposed a galloping bluff body with Y-shaped attachments where the power output of 0.576 mW can be obtained for $R = 2$ MΩ at a wind speed of ≈1.9 m s^{-1}. Moreover, a triboelectric-based energy harvester, proposed by Zhao et al.,[45] can produce a maximum power of 0.196 mW at a wind speed of 6 m s^{-1}. Tian et al.,[46] furthermore, introduced an airfoil-based energy harvester which can produce an output power of 3.382 mW at a wind speed of 14 m s^{-1}. Another energy harvester configuration can operate at a wind speed range of 2.1–15.4 m s^{-1} and can produce an output power of ≈0.090 mW.[47] Additionally, the optimum power of the system with $\theta = 0°$ is observed at ≈200 kΩ and the highest power of the harvester with $\theta = 55°$ occurs at around 450 kΩ. Furthermore, the effect of the variation in the angle of attack seems to be negligible for $\theta = 0°$ and $\theta = 55°$. However, this effect is apparent for $\theta = 180°$ where the maximum power is attained at $\alpha = 0°$ and the minimum one is seen at $\alpha = 20°$.

The power curves obtained for every harvester geometry examined with various apical angles are also presented in **Figure 12** in

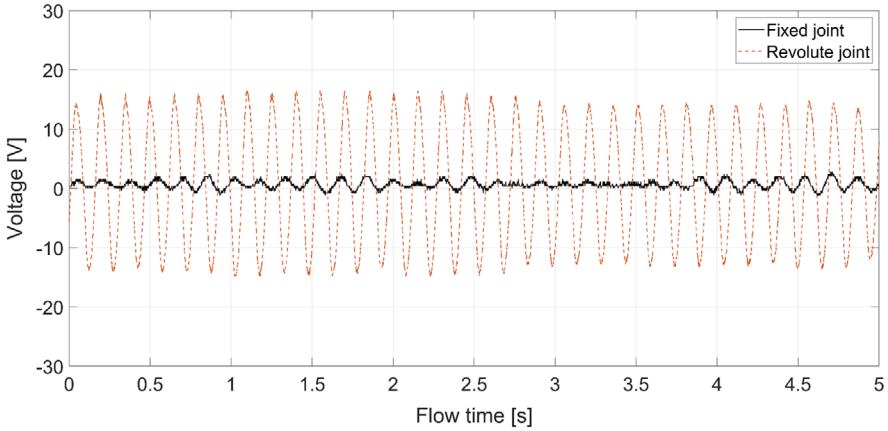

Figure 10. The comparison of the voltages produced by fixed and revolute joints at $\theta = 0°$.

© 2023 Wiley-VCH GmbH

21944296, 0, Downloaded from https://onlinelibrary.wiley.com/doi/10.1002/ente.202300579 by Bilecik Seyh Edebali, Wiley Online Library on [22/08/2023]. See the Terms and Conditions (https://onlinelibrary.wiley.com/terms-and-conditions) on Wiley Online Library for rules of use; OA articles are governed by the applicable Creative Commons License

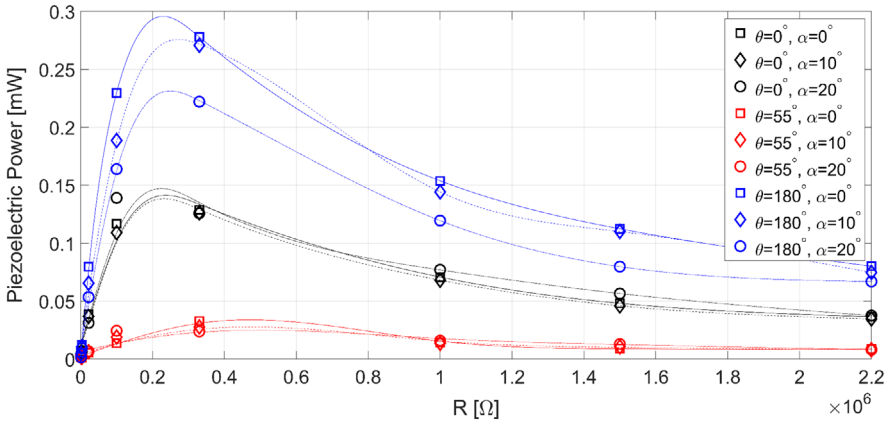

Figure 11. The variation of the power curves for $\theta = 0°$, 55°, 180° and at $\alpha = 0°$, 10°, 20° with the application of resistor values varying between 1 kΩ and 2200 kΩ.

the 3D form. In this figure, the base axes represent the apical angle θ and the electrical resistance R where the vertical axis describes the piezoelectric power generated in the unit of milliwatt. This plot markedly reveals that the highest power produced by this proposed system can be obtained at $\theta = 180°$ and for $R = 200\,\text{k}\Omega$, approximately. Moreover, there is another region which can be used for power generation that is between $\theta = 0°$–60° and $R = 1$–1000 kΩ. Furthermore, the power outputs of the proposed harvester systems with 10° and 20° angles of attack are comparable to the one produced by 0° angle of attack.

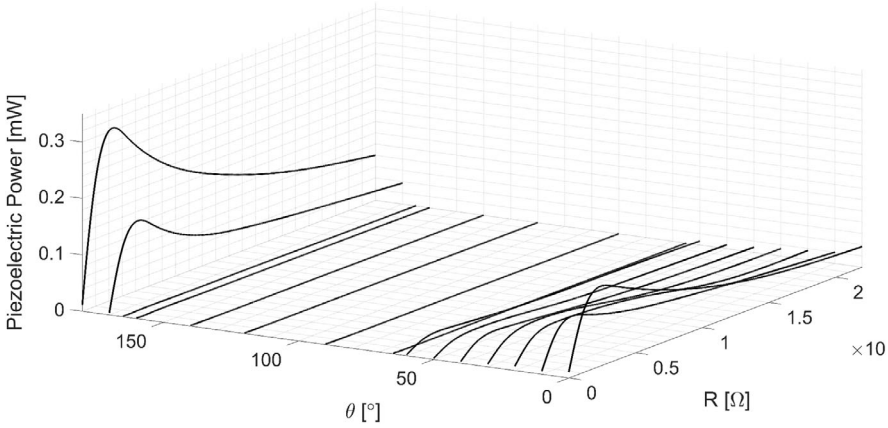

Figure 12. The variation of the power curves for $\theta = 0°$–180° and at $\alpha = 0°$ with the application of electrical resistance varying between 1 kΩ and 2200 kΩ.

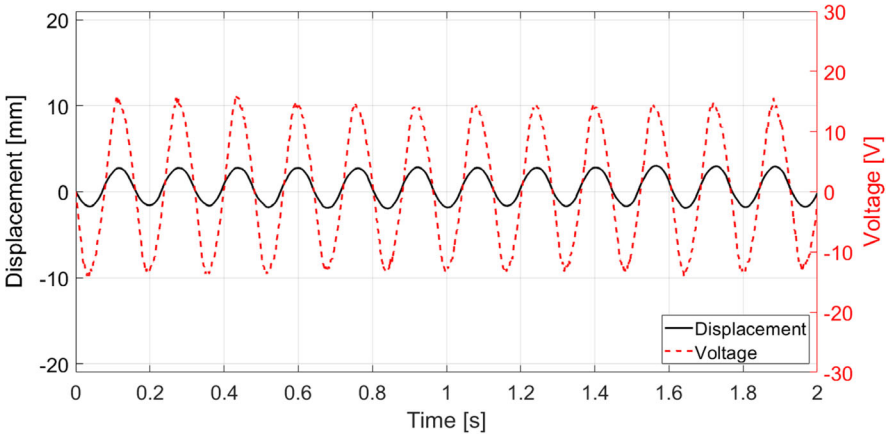

Figure 13. Displacement and voltage values obtained for $\theta = 0°$ and $\alpha = 0°$.

© 2023 Wiley-VCH GmbH

21944296, 0, Downloaded from https://onlinelibrary.wiley.com/doi/10.1002/ente.202300579 by Bilecik Seyh Edebali, Wiley Online Library on [22/08/2023]. See the Terms and Conditions (https://onlinelibrary.wiley.com/terms-and-conditions) on Wiley Online Library for rules of use; OA articles are governed by the applicable Creative Commons License

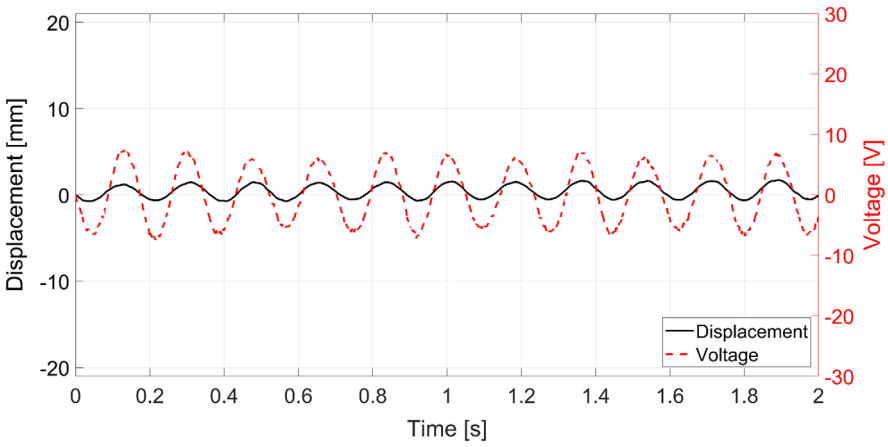

Figure 14. Displacement and voltage values obtained for $\theta = 55°$ and $\alpha = 0°$.

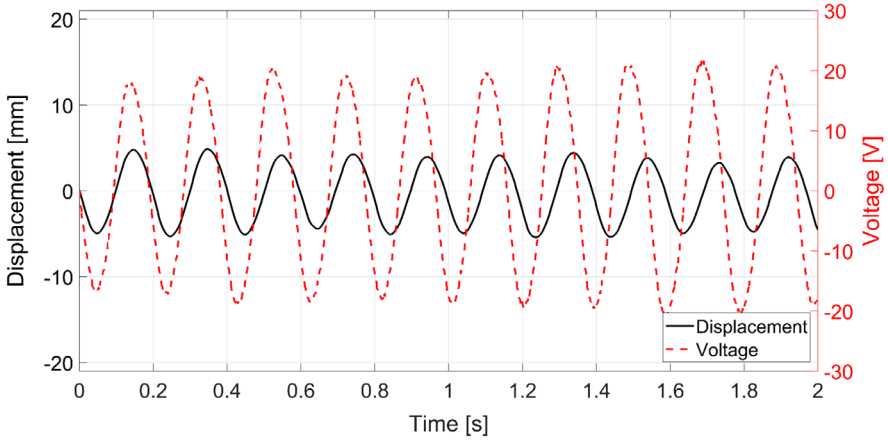

Figure 15. Displacement and voltage values obtained for $\theta = 180°$ and $\alpha = 0°$.

This reveals that although the symmetrical flow starts to break down at these angles of attack, it is still possible to benefit from such systems with most probably the additional degree of freedom by means of the revolute joint.

Figure 13–15 compare the displacement and raw voltage values acquired simultaneously for $\theta = 0°$, $\theta = 55°$, and $\theta = 180°$, respectively, at the zero angle of attack. These displacement values were obtained by means of the laser sensor positioned accordingly to record the oscillations of the cantilever beam that holds the V-shape harvesters. Due to the fact that the laser was pointed directly on the piezoelectric patch attached to the beam, these displacement data instantaneously correspond to the produced voltage by the patch. This case can be observed from these figures where the oscillations coincide with the peak voltages produced by the bending motion of the piezoelectric patch.

5. Conclusion

This study benefits from the simply designed experimental rig to investigate the behavior of the V-shape geometries with various apical angles as energy harvesters, which are attached to a cantilever beam with a revolute joint.

First, a suitable wind speed of $10\ \mathrm{m\ s^{-1}}$ for the main experiments was revealed, which corresponds to a Reynolds number of 3.16×10^4. This wind speed rather provides an instant oscillation of the system.

Following this initial consideration, RMS values of voltages were acquired and results clearly display that there is an unproductive region of the apical angle for $\approx 65° < \theta < 165°$. On the other hand, the harvester geometries with the apical angles of $\theta \approx 0°$, 10°, 170°, and 180° appear to be the most effective models in terms of their capability of electricity production.

One of the most crucial advantages of the proposed system is that it is not prone to the direction of the incoming airflow. In fact, the current experiments recommend that the angle of attack up to 20° may be beneficial in terms of the productivity of the harvester system. The V-shape harvester with the apical angle of $\theta = 60°$, for instance, can provide higher voltage when the angle of attack is set to $\alpha = 20°$ rather than $\alpha = 0°$.

Furthermore, V-shape harvester geometries are also attached to the cantilever beam with a fixed support for comparison.

© 2023 Wiley-VCH GmbH

21944296, 0, Downloaded from https://onlinelibrary.wiley.com/doi/10.1002/ente.202300579 by Bilecik Seyh Edebali, Wiley Online Library on [22/08/2023]. See the Terms and Conditions (https://onlinelibrary.wiley.com/terms-and-conditions) on Wiley Online Library for rules of use; OA articles are governed by the applicable Creative Commons License

Effective cases, such as $\theta = 0°$ and 180°, were preferred for this comparison and the results show that the harvesters with revolute joints are superior to the ones with fixed joints.

Moreover, the maximum power is acquired at $\theta = 180°$ and for $R = 200\,k\Omega$, approximately. Additionally, another productive region is observed between $\theta = 0°$–60° and $R = 1$–$1000\,k\Omega$ in the 3D representation of the power curves.

Finally, the displacement of the piezoelectric patch is provided in comparison with the voltage output at $\alpha = 0°$ and for $\theta = 0°$, 55°, and 180°. It is observed that the galloping motion of the cantilever beam and thus the piezoelectric patch coincide with the maximum amplitudes of the produced voltage readings.

Subsequent numerical studies may be carried out to shed light on the insights of the appearance of the vortex shedding in accordance with the V-shape harvester at various apical angles. By this means, a better harvester model may be revealed, which has a very particular apical angle.

Acknowledgements

This research did not receive any specific grant from funding agencies in the public, commercial, or not-for-profit sectors.

Conflict of Interest

The authors declare no conflict of interest.

Data Availability Statement

The data that support the findings of this study are available from the corresponding author upon reasonable request.

Keywords

energy harvesting, flow-induced vibrations, parametric optimization, piezoelectricity

Received: May 29, 2023
Revised: July 25, 2023
Published online:

[1] X. Ma, S. Zhou, *Energy Convers. Manage.* **2022**, *254*, 115223.
[2] S. Panda, S. Hajra, K. Mistewicz, P. Inna, M. Sahu, P. M. Rajaitha, H. J. Kim, *Nano Energy* **2022**, *100*, 107514.
[3] Q. Zhang, Z. Liu, X. Jiang, Y. Peng, C. Zhu, Z. Li, *Sustainable Energy Technol. Assess.* **2022**, *53*, 102591.
[4] S. A. Kouritem, M. A. Al-Moghazy, M. Noori, W. A. Altabey, *Mech. Syst. Signal Process.* **2022**, *181*, 109500.
[5] Y. Cao, J. Li, A. Sha, Z. Liu, F. Zhang, X. Li, *J. Cleaner Prod.* **2022**, *369*, 133287.
[6] F. Hao, B. Wang, X. Wang, T. Tang, Y. Li, Z. Yang, J. Lu, *Nano Energy* **2022**, *103*, 107823.
[7] Y. Lo, Y. Shu, *Mech. Syst. Signal Process.* **2022**, *177*, 109123.
[8] N. Sezer, M. Koç, *Nano Energy* **2021**, *80*, 105567.
[9] Y. Yu, Y. Liu, *J. Fluids Struct.* **2016**, *65*, 381.
[10] J. Carlos De Marqui, A. Erturk, *J. Intell. Mater. Syst. Struct.* **2013**, *24*, 846.
[11] F. C. Bolat, S. Basaran, S. Sivrioglu, *Mech. Syst. Signal Process.* **2019**, *133*, 106246.
[12] H. Liu, H. Fu, L. Sun, C. Lee, E. M. Yeatman, *Renewable Sustainable Energy Rev.* **2021**, *137*, 110473.
[13] L. C. Zhao, H. X. Zou, Y.-J. Zhao, Z. Y. Wu, F. R. Liu, K. X. Wei, W. M. Zhang, *Appl. Energy* **2022**, *314*, 118983.
[14] S. Yang, P. Tang, Y. Huang, Z. Du, J. Fan, G. Xiao, *Energy Technol.* **2023**, *11*, 2201003.
[15] R. Zheng, G. Li, J. Chen, C. Ning, X. Yu, C. Jiang, *Energy Technol.* **2023**, *11*, 2201253.
[16] K. Yang, A. Abdelkefi, X. Li, Y. Mao, L. Dai, J. Wang, *Energy Convers. Manage.* **2021**, *238*, 114174.
[17] M. Zhang, C. Zhang, A. Abdelkefi, H. Yu, O. Gaidai, X. Qin, H. Zhu, J. Wang, *Ocean Eng.* **2021**, *235*, 109378.
[18] J. Wang, Y. Zhang, M. Liu, G. Hu, *Int. J. Mech. Sci.* **2023**, *242*, 108016.
[19] J. Wang, L. Geng, L. Ding, H. Zhu, D. Yurchenko, *Appl. Energy* **2020**, *267*, 114902.
[20] J. Wang, L. Sheng, L. Ding, *Ocean Eng.* **2023**, *271*, 113781.
[21] J. Wang, D. Yurchenko, G. Hu, L. Zhao, L. Tang, Y. Yang, *Appl. Phys. Lett.* **2021**, *119*, 100502.
[22] A. Mehmood, A. Abdelkefi, M. Hajj, A. Nayfeh, I. Akhtar, A. Nuhait, *J. Sound Vib.* **2013**, *332*, 4656.
[23] H. Li, C. Tian, Z. D. Deng, *Appl. Phys. Rev.* **2014**, *1*, 041301.
[24] M. Koç, Ç. E. D. Dönmez, L. Paralı, A. Sarı, S. Aktürk, *J. Mater. Sci. Mater. Electron.* **2022**, *33*, 8048.
[25] C. García-Baena, J. Jiménez-González, C. Gutiérrez-Montes, C. Martínez-Bazán, *J. Fluids Struct.* **2021**, *100*, 103194.
[26] J. Wang, C. Zhang, S. Gu, K. Yang, H. Li, Y. Lai, D. Yurchenko, *Aerosp. Sci. Technol.* **2020**, *103*, 105898.
[27] F. R. Liu, H. X. Zou, W. M. Zhang, Z. K. Peng, G. Meng, *Appl. Phys. Lett.* **2018**, *112*, 233903.
[28] M. Rezaei, R. Talebitooti, *Int. J. Mech. Sci.* **2019**, *163*, 105135.
[29] H. Kim, J. Lee, J. Seok, *Energy Convers. Manage.* **2022**, *266*, 115849.
[30] A. G. A. Muthalif, M. Hafizh, J. Renno, M. Paurobally, *Energy Convers. Manage.* **2022**, *256*, 115371.
[31] J. Wang, C. Zhang, G. Hu, X. Liu, H. Liu, Z. Zhang, R. Das, *Energy* **2022**, *253*, 124175.
[32] V. Tamimi, J. Wu, S. Naeeni, S. Shahvaghar-Asl, *Appl. Energy* **2021**, *281*, 116092.
[33] Z. Yan, G. Shi, J. Zhou, L. Wang, L. Zuo, T. Tan, *Energy Convers. Manage.* **2021**, *249*, 114820.
[34] J. Wang, S. Sun, G. Hu, Y. Yang, L. Tang, P. Li, G. Zhang, *Energy Convers. Manage.* **2021**, *243*, 114414.
[35] Z. Chen, M. M. Alam, B. Qin, Y. Zhou, *Appl. Energy* **2020**, *278*, 115737.
[36] H. Zhu, T. Tang, T. Zhou, M. Cai, O. Gaidai, J. Wang, *Energy* **2021**, *236*, 121484.
[37] J. Wang, C. Zhang, D. Yurchenko, A. Abdelkefi, M. Zhang, H. Liu, *Energy* **2022**, *239*, 122203.
[38] M. Bryant, E. Wolff, E. Garcia, *Smart Mater. Struct.* **2011**, *20*, 125017.
[39] M. Bryant, E. Wolff, E. Garcia, *Proc. SPIE, 79770S*, San Diego, California, United States, April **2011**.
[40] M. Özkan, O. Erkan, S. Basaran, F. C. Bolat, *J. Phys. D: Appl. Phys.* **2022**, *56*, 024002.
[41] Y. C. Shu, I. C. Lien, *Smart Mater. Struct.* **2006**, *15*, 1499.
[42] A. Abdelkefi, M. R. Hajj, A. H. Nayfeh, *Smart Mater. Struct.* **2013**, *22*, 015014.

© 2023 Wiley-VCH GmbH

21944296, 0, Downloaded from https://onlinelibrary.wiley.com/doi/10.1002/ente.202300579 by Bilecik Seyh Edebali, Wiley Online Library on [22/08/2023]. See the Terms and Conditions (https://onlinelibrary.wiley.com/terms-and-conditions) on Wiley Online Library for rules of use; OA articles are governed by the applicable Creative Commons License

[43] Y. D. Selyutskiy, *Appl. Math. Modell.* **2019**, *67*, 449.
[44] J. Wang, S. Zhou, Z. Zhang, D. Yurchenko, *Energy Convers. Manage.* **2019**, *181*, 645.
[45] C. Zhao, G. Hu, Y. Yang, *Mech. Syst. Signal Process.* **2022**, *177*, 109185.
[46] H. Tian, X. Shan, H. Cao, T. Xie, *Mech. Syst. Signal Process.* **2022**, *162*, 108065.
[47] Z. Lai, J. Wang, C. Zhang, G. Zhang, D. Yurchenko, *Energy Convers. Manage.* **2019**, *199*, 111993.

© 2023 Wiley-VCH GmbH

21944296, 0, Downloaded from https://onlinelibrary.wiley.com/doi/10.1002/ente.202300579 by Bilecik Seyh Edebali, Wiley Online Library on [22/08/2023]. See the Terms and Conditions (https://onlinelibrary.wiley.com/terms-and-conditions) on Wiley Online Library for rules of use; OA articles are governed by the applicable Creative Commons License